

Error boundedness of Correction Procedure via Reconstruction / Flux Reconstruction

Philipp Öffner

April 2, 2022

We study the long time error behaviour of correction procedure via reconstruction / flux reconstruction methods to hyperbolic conservation laws. We show that not only the choice of the numerical flux (upwind or central) affects the growth rate and asymptotic value of the error, but also that the selection of bases (Gauß-Lobatto or Gauß-Legendre) is even more important. Using Gauß-Legendre basis, the error reaches the asymptotic value faster and to a lower value than by using Gauß-Lobatto basis. Also the differences in the error caused by the numerical flux is not essential for low resolution computations in the Gauß-Legendre case. This behaviour is best seen if a particular FR scheme is investigated which has a strong connection to the Discontinuous Galerkin framework, but holds also for other flux reconstruction schemes with low order resolution computations.

1 Introduction

There exist plenty of examples in the literature, where stable approximations of hyperbolic conservation laws demonstrate a linear error growth (or nearly linear growth) in time, even though stability of the numerical schemes should guarantee that the solution remains bounded, see [6, 10, 20]. The reason behind this is the following: The error equation for the time variation contains a forcing term generated by the approximation or truncation errors and this forcing term can trigger the unbounded growth of the error.

Simultaneously, there are other examples, where the temporal error growth is bounded [1, 14] and finally, in [18] the author gives an explanation under what conditions the error is or is not bounded in time. The author works with SBP-SAT (Summation-by-Parts/Simultaneous-Approximation-Term) finite difference approximation and summarises that the error behaviour depends only on the choice of boundary procedure of the problem.

If one catches the waves in cavities or in periodic boundary conditions, linear growth is observed like it is investigated in [10], whereas for inflow-outflow problems one obtains boundedness. In other words, if an appropriate boundary approach (sufficiently dissipative) is applied, the error is bounded. In this framework the error behaviour does not depend on the internal discretisation. In [16], the authors analyse the long time behaviour of the error for the discontinuous Galerkin spectral element methods (DGSEM). They confirm the conclusion from [18] that the bounded error property is due to the fact of dissipative boundary conditions, but different from [18], in the DGSEM framework the internal approximation has indeed an influence on the behaviour of the error. The choice of the numerical flux (upwind or central) is essential for the magnitude of the error and the speed at which the asymptotic error is reached. With the upwind flux one obtains better results.

In this paper we examine the long time error behaviour for recent correction procedure via reconstruction (CPR) / flux reconstruction (FR) method. The CPR/FR is a unifying framework for several high-order methods such as discontinuous Galerkin (DG), spectral difference (SD) and spectral volume (SV) methods

and also includes by a special choice of the nodal basis and the correction matrix the DGSEM of [16]. Here, we investigate not only the numerical flux, but also the selection of nodal bases (Gauß-Legendre and Gauß-Lobatto). We recognise that the selection of the flux function is less important as the choice of the nodal bases for the error behaviour. Using Gauß-Legendre basis in the approximation, the error is lower than in the Gauß-Lobatto case and the speed of attaining the error asymptotic is even faster for most of the problems under consideration. The selection of the numerical flux takes less influence on the error behaviour in the Gauß-Legendre case as applying a Gauß-Lobatto basis. Our investigation leads us the conclusion that for linear problems Gauß-Legendre points are the right choice especially for low order resolutions. Our analysis extends and completes the investigation/predictions from [16] to a more general framework.

The paper is organised as follows: In the second section, we repeat the main ideas of the SBP-CPR/FR methods and demonstrate the connection between CPR/FR and the DG framework. Then, we present the model problem under consideration. In the next section 4, we extend the results from [16] to the linear stable one-parameter family of Vincent [27] and also consider in our investigation Gauß-Legendre nodes. These nodes do not contain the boundary values in one element and this yields to a further error term in our error equation. We focus on this additional error term and give an interpretation for it. We demonstrate our investigation by numerical tests in section 5, which includes also one example from [16] for comparison. We mention the limitations of our results and finally, we summarise and discuss these limitations.

2 Correction Procedure via Reconstruction/Flux Reconstruction using Summation-by-Parts operators

We will shortly repeat the main idea of CPR/FR method¹ for a scalar, one-dimensional hyperbolic conservation law

$$\partial_t u + \partial_x f(u) = 0, \quad (1)$$

equipped with adequate initial and boundary conditions. The domain $\Omega \subset \mathbb{R}$ is split into disjoint open intervals $\Omega_i \subset \Omega$ such that $\bigcup_i \overline{\Omega_i} = \Omega$. The FR method is a semidiscretisation applying a polynomial approximation on elements. Each element Ω_i is transferred onto a standard element, which is in our case simply $(-1, 1)$. All calculations are conducted within this standard element. Let \mathbb{P}_N be the space of polynomials of degree $\leq N$, $-1 \leq \zeta_i \leq 1$ are interpolation points in $[-1, 1]$ and $\mathbb{I}^N : \mathbf{L}^2(-1, 1) \rightarrow \mathbb{P}_N(-1, 1)$ be the interpolation operator. The solution u is approximated by a polynomial $U \in \mathbb{P}_N$ and in the basic formulation a nodal Lagrange basis is employed. The coefficients \underline{u} of u are given by the nodal values $\underline{u}_i = u(\zeta_i), i \in \{0, \dots, N\}$. It can be written as

$$u \approx U = \sum_{i=0}^N \underline{u}_i l_i(\xi), \quad (2)$$

where $l_i(\xi)$ is the i -th Lagrange interpolation polynomial that satisfies $l_j(\xi_j) = \delta_{ij}$. The flux $f(u)$ is also approximated by a polynomial, where the coefficients are given by $\underline{f}_i = f(\underline{u}_i) = f(u(\zeta_i))$. We apply a discrete derivative matrix \underline{D} on \underline{f} . The divergence is $\underline{D}\underline{f}$. Since the solutions will probably have discontinuities across elements, we will have this in the discrete flux, too. In order to avoid this problem, we introduce a numerical flux $\underline{f}^{\text{num}}$ and also a correction term \underline{C} at the boundary nodes [25]. Hence, the FR method reads

$$\partial_t \underline{u} = -\underline{D}\underline{f} - \underline{C} \left(\underline{f}^{\text{num}} - \underline{R}\underline{f} \right), \quad (3)$$

where the restriction matrix \underline{R} performs interpolation to the boundary. A general choice of the correction matrix \underline{C} recovers the linearly stable flux reconstruction methods of [27, 28], as described by [25].

The numerical flux $\underline{f}^{\text{num}}$ computes a common flux on the boundary using values from both neighbouring elements. With respect to a chosen basis, the scalar product approximating the L^2 scalar product is represented by a matrix \underline{M} and integration with respect to the outer normal by \underline{B} . Finally, all operators are

¹For the rest of this work, we call them FR method.

introduced and they have to fulfil the SBP property

$$\underline{\underline{M}} \underline{\underline{D}} + \underline{\underline{D}}^T \underline{\underline{M}} = \underline{\underline{R}}^T \underline{\underline{B}} \underline{\underline{R}}, \quad (4)$$

in order to mimic integration by parts on a discrete level

$$\underline{\underline{u}}^T \underline{\underline{M}} \underline{\underline{D}} \underline{\underline{v}} + \underline{\underline{u}}^T \underline{\underline{D}}^T \underline{\underline{M}} \underline{\underline{v}} \approx \int_{\Omega} u (\partial_x v) + \int_{\Omega} (\partial_x u) v = u v|_{\partial\Omega} \approx \underline{\underline{u}}^T \underline{\underline{R}}^T \underline{\underline{B}} \underline{\underline{R}} \underline{\underline{v}}. \quad (5)$$

Different bases can be used like nodal Gauß-Legendre / Gauß-Lobatto-Legendre or modal Legendre bases, as described in [26]. As an example, in the standard element $[-1, 1]$ the SBP-FR method for the linear advection equation can be formulated as

$$\underline{\underline{u}}_t + \underline{\underline{D}} \underline{\underline{u}} + \underline{\underline{C}} \left(f^{\text{num}} - \underline{\underline{R}} \underline{\underline{u}} \right) = 0. \quad (6)$$

The canonical choice for the correction matrix is

$$\underline{\underline{C}} = \underline{\underline{M}}^{-1} \underline{\underline{R}}^T \underline{\underline{B}}, \quad (7)$$

which is a generalisation of SATs used in finite difference methods and corresponds to a strong form of the discontinuous Galerkin method [15].

We will apply this close connection several times in this paper. Therefore, we repeat the main aspect and present one example for a better understanding.

Different from the DG framework, FR schemes use in their discretisations of (1) no weak /variational or integral form. The differential form (3) is applied. The main idea of the FR schemes is that the numerical fluxes at the boundaries are corrected by correction functions in such manner, that basic properties like conservation hold. In [11] it is described how to embed the DG method in the FR framework and vice versa. The application of Radau polynomials as correction functions is essential. We present the following example from [11].

Example 2.1. We are considering the linear advection equation

$$u_t + a u_x = 0, \text{ where } a > 0. \quad (8)$$

Let $c(x) = c_{LB}(x)$ be left Radau polynomial of degree N on $I = [-1, 1]$. The Radau polynomials fulfil $c(-1) = 1$ and $c(1) = 0$. As the space of test functions we choose polynomials p of degree N such that $\frac{dp}{dx}$ is orthogonal to c . Here, the FR approach distinguishes from standard DG approach where the space $\mathbb{P}_{N-1}(I)$ is considered. The FR discretisation of (8) using the local coordinate ξ reads like

$$\frac{\Delta x_l}{2} (u_l)_t + \underbrace{\left(f_l(\xi) + \left(f_{up,l-1/2}^{\text{num}}(-1) - f_l(-1) \right) c(\xi) \right)}_{=:(F_l)_\xi} = 0, \quad (9)$$

where u_l , f_l are polynomials and approximate u and f . $f_{up,l-1/2}^{\text{num}}$ is the upwind flux. Multiplying by a test function p (polynomial of degree N) and integrating over I casts (9) in the DG framework. We obtain

$$\int_I \left(\frac{\Delta x_l}{2} (u_l)_t + (F_l)_\xi \right) p(\xi) d\xi = 0. \quad (10)$$

Applying integration-by-parts twice and using the properties of c yields

$$\begin{aligned} \int_I ((F_l)_\xi) p(\xi) d\xi &= (f_l p)(1) - (f_l p)(-1) - \int_I f_l(\xi) p_\xi(\xi) d\xi - \left(f_{up,l-1/2}^{\text{num}}(-1) - f_l(-1) \right) p(-1) \\ &\quad - \int_I \left(f_{up,l-1/2}^{\text{num}}(-1) - f_l(-1) \right) c(\xi) p_\xi(\xi) d\xi \end{aligned} \quad (11)$$

With $\int_I c(\xi) p_\xi(\xi) d\xi = 0$ and $f_{up,l+1/2}^{\text{num}} = f_l(1)$, (11) we obtain

$$\int_I ((F_l)_\xi) p(\xi) d\xi = f_{up,l+1/2}^{\text{num}}(1)p(1) - f_{up,l-1/2}^{\text{num}}(-1)p(-1) - \int_I f_l(\xi) p_\xi d\xi.$$

Combining the above equation with (10), we get the following DG form

$$\frac{d}{dt} \int_I \frac{\Delta x_l}{2} u_l p(\xi) d\xi + [f_{up}^{\text{num}} p]_{\partial I} - \int_I f_l(\xi) p_\xi(\xi) d\xi = 0.$$

This example demonstrates well the connection between the DG and FR framework. For a more detailed overview we strongly recommend the paper [12] and references therein. Besides conservation, one central point is (linear) stability of our numerical schemes, the discrete analogue to well-posedness.

Decisive here is the choice of correction functions (correction matrix). [27, 28] investigated this and the authors derive linear stable FR schemes depending on these correction functions. Their study is based on an idea of Jameson [13], where he shows linear stability using the equivalence of norms in finite dimensional vector spaces and applies broken Sobolev norms involving derivatives instead of using a regular \mathbf{L}^2 -norm. He utilises

$$||u||_{H_c}^2 := \int u^2 + \tilde{c}(u^{(p)})^2 dx, \quad (12)$$

where p represents the order of accuracy and depends therefore on N . Simultaneously, \tilde{c} depends on the chosen correction function. In order to guarantee that (12) defines a norm, \tilde{c} has to be bounded from below. In [27] the authors investigate correction functions of the form

$$c_L(x) = \frac{(-1)^p}{2} \left[L_p - \left(\frac{\lambda_p L_{p-1} + L_{p+1}}{1 + \lambda_p} \right) \right], \quad c_R(x) = \frac{1}{2} \left[L_p + \left(\frac{\lambda_p L_{p-1} + L_{p+1}}{1 + \lambda_p} \right) \right], \quad (13)$$

where L_p is the p -Legendre polynomial and $\lambda_p = \frac{c(p+1)2^{2p}(p!)^4}{((2p)!p!)^2}$ is a term with the free parameter² c . The different selection of c yields to varying numerical methods and in Table 1 three different schemes are given. c can theoretically tend to infinity as it is described and analysed in [27]. Nevertheless, we exclude this case based on the fact that we loss significant accuracy for $c \rightarrow \infty$ in our FR schemes. We even go one step further and suppose that with increased p , c has to decrease rapidly to zero (or be zero). This includes the most famous schemes written in the following table from [27].

p	c_{SD}	c_{Hu}	c_{DG}
2	4/135	1/15	0
3	1/1050	8/4725	0
4	8/496125	1/39690	0
5	1/5893965	12/49116375	0

Table 1: Values of c to get different numerical schemes

Remark 2.2. In other words, linear stable FR schemes are obtain if the correction functions (13) are used and the free parameter c is bounded from below to guarantee that by (12) a norm is introduced [13, 27, 28]. For $c = 0$ we are again in the classical DG framework and the regular \mathbf{L}^2 -norm is measured. As it is already known [5, 27, 28], the most accurate results are obtained if $c = 0$.

We apply SBP operators and consider fully discrete norms in our approach, this is slight different from [13, 27, 28], where continuous integral norms are applied. Nevertheless, the same schemes are investigated [25].

²The only difference between \tilde{c} and c is some scaling term for the intervals under consideration, see [27] for details.

3 Model problem

To analyse the long time error behaviour of SBP-CPR/FR method, we study analogue to [16, 18] the scalar linear advection equation with non-periodic boundary conditions

$$\begin{aligned} u_t + u_x &= 0, \quad x \in [0, L], \quad t \geq 0 \\ u(t, 0) &= g(t), \\ u(0, x) &= u_0(x). \end{aligned} \tag{14}$$

We assume also that the initial and boundary values are chosen in such way that $u(t, x) \in H_c^m(0, L)$ for $m > 1$ and that $\|u\|_{H_c^m}$ is uniformly bounded in time. Like it is described in [16], such conditions are physically meaningful, because they describe problems where the boundary input is, for instance, sinuoidal. In our numerical tests in section 5, we will present also an example, where these conditions are not fulfilled, see subsection 5.2. Here, H_c^m derives the classical Sobolev norm together with our broken norm depending on c . In total, the highest derivative is $m + p$ and since p tends to infinity, c tends to zero rapidly cause of our assumption. This fact will be important later on in this paper, since we are able to negligible some of the error terms and cancel them out. As it is well-known, the boundary conditions of (14) has an essential impact on the solution and in [19], the author also shows that a correct implementation of the boundary conditions is essential for well-posedness. We shortly give the following example from [16] in the DG context whereas for general FR schemes the analysis can be found in [27, 28].

Example 3.1. Here, the energy of the solution u of the initial boundary value problem (14) is measured by the regular L^2 -norm $\|u\|^2 = \int_0^L u^2 dx$. Focusing on the weak formulation of the advection equation (14), we multiply with a test function $\varphi \in C^1(0, L)$ and integrate over the domain. We get

$$\int_0^L u_t \varphi dx + \int_0^L u_x \varphi dx = 0.$$

$\varphi = u$ and integration by parts yield

$$\frac{1}{2} \frac{d}{dt} \|u\|^2 = - \int_0^L u u_x dx = g^2(t) - u^2(L, t).$$

Integration in time over an interval $[0, T]$ leads to

$$\|u(T)\|^2 + \int_0^T u^2(L, t) dt = \|u_0\|^2 + \int_0^T g^2(t) dt. \tag{15}$$

We see that the energy at time T can be expressed by the initial energy plus the energy added at the left side through the boundary condition minus the energy, which we loss through the right side. Therefore, the selection of the boundary conditions is substantial and the numerical approximation has to imitate this.

4 Long time error behaviour for SBP-FR

Before we start with our analysis about stability of the SBP-FR methods and derive the error equations, we give an overview about the notation and some basic approximation properties which will be used later in this section. We analyse stability in the semidiscrete sense. Therefore, we divide all the interval in elements $e^k = [x^{k-1}, x^k]$, $k = 1, \dots, K$, whereas the x^k are the element boundaries with $x^0 = 0$ and $x^K = L$. $\frac{\Delta x_k}{2} = \frac{x^k - x^{k-1}}{2}$ is a transformation factor, because we calculate everything in our standard element $(-1, 1)$. Like it was explained in section 2, we transform every element to our standard element and use a SBP-FR method. We investigate both Gauß-Lobatto and Gauß-Legendre quadrature. We also provide estimations for a modal Legendre basis. Here, we would assume exact integration. Then, the analysis for modal Legendre basis is similar to Gauß-Legendre and can be transferred with these estimations.

We can define the discrete inner product by

- Gauß-Lobatto

$$(U, V)_N := \sum_{j=0}^N U(\xi_j) V(\xi_j) \omega_j = \int_{-1}^1 UV \, d\xi \quad \forall UV \in \mathbb{P}^{2N-1}, \quad (16)$$

- Gauß-Legendre

$$(U, V)_N := \sum_{j=0}^N U(\xi_j) V(\xi_j) \omega_j = \int_{-1}^1 UV \, d\xi \quad \forall UV \in \mathbb{P}^{2N+1}. \quad (17)$$

We choose the numerical flux to have the form

$$f^{\text{num}}(U_L, U_R) = \frac{U_L + U_R}{2} - \frac{\sigma}{2}(U_R - U_L), \quad \sigma \in [0, 1],$$

where U_L, U_R are the states on the left and right boundaries. For $\sigma = 0$ we get the central flux and for $\sigma = 1$ the upwind flux is obtained. We analyse the time behaviour of the error. The error is given by $E^k := u(x(\xi), t) - U^k(\xi, t)$. We can split the error in two parts:

$$E^k = \underbrace{(\mathbb{I}^N(u)^k - U^k)}_{=: \varepsilon_1^k \in \mathbb{P}} + \underbrace{(u - \mathbb{I}^N(u)^k)}_{=: \varepsilon_p^k}. \quad (18)$$

We will investigate discrete norms in this context using the discrete inner products (16) and (17). The global norm, which depends only on t , is defined by

$$\|U(t)\|_N^2 := \sum_{k=1}^K \frac{\Delta x_k}{2} \|U^k(t)\|_N^2, \quad (19)$$

and $U(0)$ is the interpolant of the initial condition u_0 . With the triangle inequality, we can bound the error (18) by

$$\|E^k\|_N^2 \leq \|\varepsilon_1^k\|_N^2 + \|\varepsilon_p^k\|_N^2. \quad (20)$$

ε_p^k is the interpolation error, which is the sum of the series truncation error and the aliasing error³. As it was already described in [4, 7, 9, 21, 22], the continuous norms converge spectrally fast for the different bases under consideration. We denote by

$$|u|_{H^{m;N}(-1,1)} := \left(\sum_{j=\min(m,N+1)}^m \|u^{(j)}\|_{L^2(-1,1)}^2 \right)^{\frac{1}{2}}$$

the seminorms of the Sobolev space $H^m(-1, 1)$ and P_N is the projection operator of the truncated Legendre series⁴. We get:

- Gauß-Lobatto/Gauß-Legendre points

$$\|u - \mathbb{I}(u)\|_{L^2(-1,1)} \leq CN^{-m} |u|_{H^{m;N}(-1,1)}; \quad (21)$$

- Legendre basis

$$\|u - P_N(u)\|_{L^2(-1,1)} \leq CN^{-m} |u|_{H^{m;N}(-1,1)}; \quad (22)$$

where C depends on m . The generalisation of these formulas (21) and (22) for $1 \leq l \leq m$ are

³If we use a modal Legendre basis in our CPR method and suppose exact integration. The interpolation operator in equation (18) can be replaced by the projection operator. The *interpolation error* is only the series truncation error. The investigation can be carried out analogously. We will provide some estimations, but not consider this case here in detail.

⁴See section 5.4.2 of [4] for detail.

- Gauß-Lobatto/Gauß-Legendre points

$$\|u - \mathbb{I}(u)\|_{H^l(-1,1)} \leq CN^{2l-\frac{1}{2}-m}|u|_{H^{m;N}(-1,1)}; \quad (23)$$

- Legendre basis

$$\|u - P_N^l(u)\|_{H^n((-1,1))} \leq CN^{n-m}|u|_{H^{m;N}(-1,1)}; \quad (24)$$

for all $0 \leq n \leq l$ and P_N^l is the orthogonal projection of u onto \mathbb{P}_N , under the inner product of $H^l(-1,1)$.

In view of our investigation, we need to consider our interpolation error not only in the standard interval $[-1,1]$, but in each element e^k . Therefore, we will transform our estimations (21)-(22) to every element. We get with the interval length $\Delta x^k = x^k - x^{k-1}$:

- Gauß-Lobatto/Gauss-Legendre⁵ points (Combination of [7, Theorem 6.6.1] and [4, Section 5.4.4])

$$\|\varepsilon_p^k\|_{H^n(e^k)} \leq C \left(\Delta x^k\right)^{n-\min\{m,N\}+\frac{1}{2}} N^{n-m+\frac{1}{2}} |u|_{H^{m;N}(e^k)}; \quad (25)$$

for $n = 0, 1$. For Gauss-Lobatto, we can delete $\frac{1}{2}$ on the right side of (25).

- Legendre basis ([4, Section 5.4.4])

$$\|u - P_N^l(u)\|_{H^n(e^k)} \leq C (\Delta x)^{n-\min\{m,N\}} N^{n-m} |u|_{H^{m;N}(e^k)}. \quad (26)$$

Now, we have introduced all notations and also the approximation estimations which we need.

Stability of the SBP-FR methods

We follow the steps from [16]. and start by repeating the main aspects of the the stability analysis of our SBP-FR methods, see [25] for details. Afterwards, we derive an error equation for the SBP-FR methods to the model problem (14). In [16] the authors investigate the long time error behaviour for the Discontinuous-Galerkin-Spectral-Element Method (DGSEM) using Gauss-Lobatto nodes. Here, we make two extensions to their investigation. First, we also consider Gauss-Legendre nodes and secondly, we also investigate the long time error behaviour of the one parameter family of Vincent et al. where the DGSEM is included⁶. Instead of using the discrete norm which is represented by $\underline{\underline{M}}$ and corresponds to the continuous \mathbf{L}^2 -norm we are applying $\underline{\underline{M}} + \underline{\underline{K}}$ analogues to [25]. The matrix $\underline{\underline{M}}$ is associated as usual with the quadrature rule given by the polynomial basis and $\underline{\underline{K}}$ is a symmetric matrix satisfying $\underline{\underline{M}} + \underline{\underline{K}} > 0$, i.e. positive definite. We are studying the change of the discrete norm $\|\underline{u}^k\|_{\underline{\underline{M}}+\underline{\underline{K}}}^2 = \underline{u}^{k,T}(\underline{\underline{M}} + \underline{\underline{K}})\underline{u}^k$ for the total energy. We multiply $\underline{\varphi}^{k,T}(\underline{\underline{M}} + \underline{\underline{K}})$ to equation (6). Here, k describes the element and T means only the transposed vector. We get

$$\frac{\Delta x_k}{2} \underline{\varphi}^{k,T}(\underline{\underline{M}} + \underline{\underline{K}}) \partial_t \underline{u}^k = -\underline{\varphi}^{k,T}(\underline{\underline{M}} + \underline{\underline{K}}) \underline{\underline{D}} \underline{u}^k - \underline{\varphi}^{k,T}(\underline{\underline{M}} + \underline{\underline{K}}) \underline{\underline{C}} \left(\underline{f}^{\text{num},k} - \underline{\underline{R}} \underline{u}^k \right) \quad (27)$$

where the numerical flux is given by $\underline{f}^{\text{num},k} = (f_L^{\text{num},k}, f_R^{\text{num},k})^T$.

By following the steps from [25] applying $\underline{\varphi}^k = \underline{u}^k$, the SBP property and assuming that $\underline{\underline{K}}\underline{\underline{D}}$ is antisymmetric, we can express the rate of change of the total energy by

$$\frac{1}{2} \frac{d}{dt} \sum_{k=1}^K \frac{\Delta x_k}{2} \|\underline{u}^k\|_{\underline{\underline{M}}+\underline{\underline{K}}}^2 = - \sum_{k=1}^K \underline{u}^{k,T} \underline{\underline{R}}^T \underline{\underline{B}} \left(\underline{f}^{\text{num},k} - \frac{1}{2} \underline{\underline{R}} \underline{u}^k \right). \quad (28)$$

⁵ A more detailed analysis can be found in [2,3].

⁶ c has to be zero or in the context of SBP operators the canonical choice (7) is used.

If we now split the sum into three parts and using the fact that the numerical flux is unique at the interface of two elements, we can rewrite⁷ (28):

$$\begin{aligned} \frac{1}{2} \frac{d}{dt} \sum_{k=1}^K \frac{\Delta x_k}{2} \|u^k\|_{M+\tilde{K}}^2 &= \frac{1}{2} \frac{d}{dt} \sum_{k=1}^K \frac{\Delta x_k}{2} \|U^k(t)\|_{M+\tilde{K}}^2 = - \sum_{k=1}^K u^{k,T} \underline{R}^T \underline{B} \left(f^{\text{num},k} - \frac{1}{2} \underline{R} u^k \right) \\ &= \frac{1}{2} g(t)^2 - \frac{1}{2} \left(U_L^1(t) - g(t) \right)^2 - \frac{1}{2} \left(U_R^K(t) \right)^2 - \frac{\sigma}{2} \sum_{k=2}^K \left(\llbracket U^k \rrbracket \right)^2, \end{aligned}$$

where U_i ($i = L, R$) describe the approximated solution (2) and the indices give the position in the elements and $\llbracket U^k \rrbracket := U_R^{k-1} - U_L^k$ is the jump. Defining the global norm corresponding to $\underline{M} + \tilde{\underline{K}}$ by

$\|U(t)\|_{\tilde{K}}^2 := \sum_{k=1}^K \frac{\Delta x_k}{2} \|U^k(t)\|_{M+\tilde{K}}^2$ and $U(0)$ is the interpolant of the initial condition u_0 . Integration from zero to T yields

$$\|U(T)\|_{\tilde{K}}^2 + \int_0^T \left(U_R^K(t) \right)^2 dt + \int_0^T \left(U_L^1(t) - g(t) \right)^2 dt + \sigma \int_0^T \sum_{k=2}^K \left(\llbracket U^k \rrbracket \right)^2 dt = \|U(0)\|_{\tilde{K}}^2 + \int_0^T g^2(t) dt,$$

which also satisfies

$$\|U(T)\|_{\tilde{K}}^2 + \int_0^T \left(U_R^K(t) \right)^2 dt \leq \|U(0)\|_{\tilde{K}}^2 + \int_0^T g^2(t) dt, \quad (29)$$

This was already proven in [25, Theorem 5], together with the fact, that our methods correspond to FR schemes, see [25] for details. For the one-parameter⁸ family of Vincent et al., the setting is

$$\tilde{\underline{K}} \underline{D} = 0, \quad \text{where } \tilde{\underline{K}} = \kappa (\underline{D}^N)^T \underline{M} \underline{D}^N, \quad (30)$$

and the selection of κ yields different numerical methods [25]. Here, κ represents c from definition (12) and the derivative matrix \underline{D} the derivatives in terms of u . Our norms under consideration are fully discrete. Nevertheless, the same schemes are analysed as in [27].

4.1 Error Equation

For the discription of the error, we follow the steps [16] and we evolve the error equation / estimation regarding the global norm $\|\cdot\|_{\tilde{K}}$. The error is given by $E^k = u(x(\xi, t) - U^k(\xi, t))$. Using (18) and the triangle inequality, we can bound the error by

$$\|E^k\|_{\tilde{K}}^2 \leq \|\varepsilon_1^k\|_{\tilde{K}}^2 + \|\varepsilon_p^k\|_{\tilde{K}}^2. \quad (31)$$

We are considering a finite dimensional normed vector space. All norms are equivalent in this vector space and this allows us to bound the discrete norm in terms of the continuous ones. Like it was already described, a kind of broken Sobolev norm is applied, where we assume that the factor c (or κ) tends rapidly to zero depending on the accuracy p of our scheme. Therefore, these terms can be neglected in our investigation. However, the first part of the continuous norms can be estimated by (21)- (26) and the interpolation error $\|\varepsilon_p^k\|_N$ decay spectrally fast.

In other words, the part of the error we have to investigate in detail is ε_1^k . This error describes the difference

⁷Details can be found in [16, 25] as well as in subsection 4.1 .

⁸The results for the multi-parameter family are similar to those about the one parameter family, since the one parameter family is contained in the extended range of schemes. In our investigation we only consider the one parameter family for simplicity.

of the interpolation of u and the the spatial approximation U . We derive now the error equation for ε_1^k . u is the solution of the continuous equation

$$\frac{\Delta x}{2}(\partial_t u, \varphi) + u\varphi \Big|_{-1}^1 - (u, \partial_\xi \varphi) = 0, \quad (32)$$

where $(u, \varphi) := \int_{-1}^1 u\varphi \, d\xi$ defines the inner product. Equation (32) can be derived from the advection equation (14) by multiplication with the test function φ , integrating over the standard element and integration-by-parts. With $\varphi \in \mathbb{P}_N \subset \mathbf{L}^2$ and $u = \mathbb{I}^N(u) + \varepsilon_p^k$, we get for the continuous equation

$$\frac{\Delta x_k}{2} \left(\partial_t \mathbb{I}^N(u)^k, \varphi^k \right) + \mathbb{I}^N(u)^k \varphi^k \Big|_{-1}^1 - (\mathbb{I}^N(u)^k, \partial_\xi \varphi^k) = -\frac{\Delta x_k}{2} \left(\partial_t \varepsilon_p^k, \varphi^k \right) - \varepsilon_p^k \varphi^k \Big|_{-1}^1 + \left(\varepsilon_p^k, \partial_\xi \varphi^k \right). \quad (33)$$

Remark 4.1. For Gauß-Lobatto nodes $\varepsilon_p^k = 0$ at the endpoints, since the interpolant is equal to the solution there. It is $\varepsilon_p^k \varphi^k \Big|_{-1}^1 = 0$.

Using integration-by-parts for $(\varepsilon_p^k, \partial_\xi^k)$ yields

$$\frac{\Delta x_k}{2} \left(\partial_t \mathbb{I}^N(u)^k, \varphi^k \right) + \mathbb{I}^N(u)^k \varphi^k \Big|_{-1}^1 - (\mathbb{I}^N(u)^k, \partial_\xi \varphi^k) = -\frac{\Delta x_k}{2} \left(\partial_t \varepsilon_p^k, \varphi^k \right) - \left(\partial_\xi (\varepsilon_p^k), \varphi^k \right). \quad (34)$$

Applying now interpolation and the discrete norm gives for the first term

$$\left(\partial_t \mathbb{I}^N(u)^k, \varphi^k \right) = \left(\partial_t \underline{\mathbb{I}^N(u)}^k, \underline{\varphi}^k \right)_{M+\tilde{K}} + \left\{ \left(\partial_t \mathbb{I}^N(u)^k, \varphi^k \right) - \left(\partial_t \underline{\mathbb{I}^N(u)}^k, \underline{\varphi}^k \right)_{M+\tilde{K}} \right\}. \quad (35)$$

Since $\varphi \in \mathbb{P}_N$, we have for the volume term

$$\begin{aligned} \left(\mathbb{I}^N(u)^k, \partial_\xi \varphi^k \right) &= \left(\underline{\mathbb{I}^N(u)}^k, \partial_\xi \underline{\varphi}^k \right)_{M+\tilde{K}} = \underline{\varphi}^k \underline{D}^T (\underline{M} + \tilde{K}) \underline{\mathbb{I}^N(u)}^k \\ &= \underline{\varphi}^k \underline{D}^T (\underline{M}) \underline{\mathbb{I}^N(u)}^k = \left(\underline{\mathbb{I}^N(u)}^k, \partial_\xi \underline{\varphi}^k \right)_N. \end{aligned} \quad (36)$$

Finally, the values of the interpolation polynomial at the boundaries of the element (-1 and 1) can be approximated by a limitation process from the left side $\mathbb{I}^N(u)^{k,-}$ and right side $\mathbb{I}^N(u)^{k,+}$. To simplify the notation we define

$$\underline{f}^{\text{num},k} \left(\mathbb{I}^N(u)^{k,-}, \mathbb{I}^N(u)^{k,+} \right) := \left(f^{\text{num}} \left(\mathbb{I}_R^N(u)^{k-1}, \mathbb{I}_L^N(u)^k \right), f^{\text{num}} \left(\mathbb{I}_R^N(u)^k, \mathbb{I}_L^N(u)^{k+1} \right) \right)^T. \quad (37)$$

We obtain for the approximation

$$\begin{aligned} \mathbb{I}^N(u)^k \varphi^k \Big|_{-1}^1 &= \underline{\varphi}^{T,k} \underline{R}^T \underline{B} \underline{f}^{\text{num},k} \left(\mathbb{I}^N(u)^{k,-}, \mathbb{I}^N(u)^{k,+} \right) \\ &\quad + \left(\varphi^k \mathbb{I}^N(u)^k \Big|_{-1}^1 - \underline{\varphi}^{T,k} \underline{R}^T \underline{B} \underline{f}^{\text{num},k} \left(\mathbb{I}^N(u)^{k,-}, \mathbb{I}^N(u)^{k,+} \right) \right). \end{aligned}$$

u is continuous ($m > 1$). Using Gauß-Lobatto points the error term in the braces is zero, because the interpolation polynomial is evaluated at these boundaries and the numerical flux is unique. For Gauss-Legendre points, we get an additional error term, which corresponds to an interpolation error (in the pointwise sense) at these end points. The numerical flux is again unique and so the error term reads

$$\varepsilon_2^k := \left\{ \left(\varphi^k \mathbb{I}^N(u)^k \Big|_{-1}^1 - \underline{\varphi}^{T,k} \underline{R}^T \underline{B} \underline{f}^{\text{num},k} \left(\mathbb{I}^N(u)^{k,-}, \mathbb{I}^N(u)^{k,+} \right) \right) \right\} \quad (38)$$

in the k -th element. Finally, using (36)-(38) in (35) we obtain

$$\begin{aligned} & \frac{\Delta x_k}{2} \left(\partial_t \underline{\mathbb{I}^N(u)}^k, \underline{\varphi}^k \right)_{M+\tilde{K}} + \underline{\varphi}^{T,k} \underline{R}^T \underline{B} f^{\text{num},k} \left(\mathbb{I}^N(u)^{k,-}, \mathbb{I}^N(u)^{k,+} \right) \\ & - \left(\left(\underline{\mathbb{I}^N(u)}^k, \partial_\xi \underline{\varphi}^k \right)_{M+\tilde{K}} = -\frac{\Delta x_k}{2} \left(\partial_t \varepsilon_p^k, \varphi^k \right) - \left(\partial_\xi(\varepsilon_p^k), \varphi^k \right) \right. \\ & \left. - \frac{\Delta x_k}{2} \left\{ \left(\partial_t \mathbb{I}^N(u)^k, \varphi^k \right) - \left(\partial_t \underline{\mathbb{I}^N(u)}^k, \underline{\varphi}^k \right)_{M+\tilde{K}} \right\} - \varepsilon_2^k. \right. \end{aligned} \quad (39)$$

Using

$$\begin{aligned} \left(\partial_t \mathbb{I}^N(u)^k, \varphi^k \right) - \left(\partial_t \underline{\mathbb{I}^N(u)}^k, \underline{\varphi}^k \right)_{M+\tilde{K}} &= \left(\underbrace{\partial_t \left(\mathbb{I}^N(u) - P_{N-1}^m \left(\mathbb{I}^N(u)^k \right) \right)}_{=: Q(u)^k}, \varphi^k \right) \\ & - \left(\partial_t \left(\underline{\mathbb{I}^N(u)}^k - P_{N-1}^m \left(\underline{\mathbb{I}^N(u)}^k \right) \right), \underline{\varphi}^k \right)_{M+\tilde{K}}, \end{aligned}$$

yields in (39)

$$\begin{aligned} & \frac{\Delta x_k}{2} \left(\partial_t \underline{\mathbb{I}^N(u)}^k, \underline{\varphi}^k \right)_{M+\tilde{K}} + \underline{\varphi}^{T,k} \underline{R}^T \underline{B} f^{\text{num},k} \left(\mathbb{I}^N(u)^{k,-}, \mathbb{I}^N(u)^{k,+} \right) - \left(\underline{\mathbb{I}^N(u)}^k, \partial_\xi \underline{\varphi}^k \right)_{M+\tilde{K}} \\ & = \frac{\Delta x_k}{2} \left(T^k(u), \varphi^k \right) + \frac{\Delta x_k}{2} \left(Q(u)^k, \underline{\varphi}^k \right)_{M+\tilde{K}} - \varepsilon_2^k. \end{aligned} \quad (40)$$

with

$$T^k(u) = - \left\{ \partial_t \varepsilon_p^k + \partial_x \varepsilon_p^k + Q(u)^k \right\}.$$

Q measures the projection error of a polynomial of degree N to a polynomial of degree $N-1$. Since u is bounded, also this value has to be bounded. Since (25) and $c \rightarrow 0$, the interpolation error ε_p^k converges in N to zero, if $m > 1$, and the Sobolev norm of the solution is uniformly bounded in time⁹. For the time derivative, we get the boundedness of the norm by the relation $\partial_t u = -\partial_x u$. ε_2^k also is bounded, because u is bounded and also continuous. For the numerical fluxes, this value describes the error between the interpolation polynomial at -1 and 1 and the numerical approximation by the numerical flux function at these boundaries. From a different perspective, this value can also be interpreted as the additional dissipation, which is added in the Gauß-Legendre case, since for Gauß-Lobatto nodes this error term is zero. We applied the SBP property (4), $\underline{C} = \left(\underline{M} + \underline{K} \right)^{-1} \underline{R}^T \underline{B}$ and the assumption (30) to equation (27) and subtract it from (40). We get with the linearity of the numerical flux an equation for the error $\varepsilon_1^k = \mathbb{I}^N(u)^k - U^k$. We obtain

$$\begin{aligned} & \frac{\Delta x_k}{2} \left(\partial_t \left(\underline{\mathbb{I}^N(u)}^k - \underline{U}^k \right), \underline{\varphi}^k \right)_{M+\tilde{K}} + \underline{\varphi}^{T,k} \underline{R}^T \underline{B} f^{\text{num},k} \left(\left(\mathbb{I}^N(u)^k - U^k \right)^-, \left(\mathbb{I}^N(u)^k - U^k \right)^+ \right) \\ & - \left(\left(\underline{\mathbb{I}^N(u)}^k - \underline{U}^k \right), \partial_\xi \underline{\varphi}^k \right)_{M+\tilde{K}} = \frac{\Delta x_k}{2} \left(T^k(u), \varphi^k \right) + \frac{\Delta x_k}{2} \left(Q(u)^k, \underline{\varphi}^k \right)_{M+\tilde{K}} - \varepsilon_2^k, \\ & \iff \frac{\Delta x_k}{2} \left(\partial_t \underline{\varepsilon}_1^k, \underline{\varphi}^k \right)_{M+\tilde{K}} + \underline{\varphi}^{T,k} \underline{R}^T \underline{B} f^{\text{num},k} \left(\left(\varepsilon_1^k \right)^-, \left(\varepsilon_1^k \right)^+ \right) - \left(\underline{\varepsilon}_1^k, \partial_\xi \underline{\varphi}^k \right)_{M+\tilde{K}} \\ & = \frac{\Delta x_k}{2} \left(T^k(u), \varphi^k \right) + \frac{\Delta x_k}{2} \left(Q(u)^k, \underline{\varphi}^k \right)_{M+\tilde{K}} - \varepsilon_2^k, \end{aligned}$$

⁹ Therefore, we need the initial and boundary conditions in the model problem (14).

where we can write for the term $\left(\underline{\varepsilon}_1^k, \partial_\xi \varphi^k\right)_{M+\tilde{K}} = \left(\underline{\varepsilon}_1^k, \partial_\xi \underline{\varphi}^k\right)_N$, because assumption (30) is fulfilled. Putting $\varphi^k = \varepsilon_1^k$, we obtain the energy equation

$$\begin{aligned} & \frac{\Delta x_k}{4} \frac{d}{dt} \|\varepsilon_1^k\|_{M+\tilde{K}}^2 + \underline{\varepsilon}_1^{T,k} \underline{R}^T \underline{B} f^{\text{num},k} \left(\left(\varepsilon_1^k\right)^-, \left(\varepsilon_1^k\right)^+ \right) - \left(\underline{\varepsilon}_1^k, \partial_\xi \underline{\varepsilon}_1^k\right)_N \\ &= \frac{\Delta x_k}{2} \left(T^k(u), \varepsilon_1^k \right) + \frac{\Delta x_k}{2} \left(\underline{Q}(u)^k, \underline{\varepsilon}_1^k \right)_{M+\tilde{K}} - \tilde{\varepsilon}_2^k, \end{aligned}$$

with $\tilde{\varepsilon}_2^k = \left(\varepsilon_1^k \mathbb{I}^N(u)^k \Big|_{-1}^1 - \underline{\varepsilon}_1^{T,k} \underline{R}^T \underline{B} f^{\text{num},k} \left(\mathbb{I}^N(u)^{k,-}, \mathbb{I}^N(u)^{k,+} \right) \right)$. Summation-by-parts yields for ε_1^k

$$\begin{aligned} \left(\underline{\varepsilon}_1^k, \partial_\xi \underline{\varepsilon}_1^k\right)_N &= \underline{\varepsilon}_1^{T,k} \underline{M} \underline{D} \underline{\varepsilon}_1^k = \underline{\varepsilon}_1^{T,k} \underline{R}^T \underline{B} \underline{R} \underline{\varepsilon}_1^k - \underline{\varepsilon}_1^{T,k} \underline{D}^T \underline{M} \underline{\varepsilon}_1^k, \\ \iff \underline{\varepsilon}_1^{T,k} \underline{M} \underline{D} \underline{\varepsilon}_1^k &= \frac{1}{2} \underline{\varepsilon}_1^{T,k} \underline{R}^T \underline{B} \underline{R} \underline{\varepsilon}_1^k, \end{aligned}$$

and we get

$$\begin{aligned} & \frac{\Delta x_k}{4} \frac{d}{dt} \|\varepsilon_1^k\|_{M+\tilde{K}}^2 + \underline{\varepsilon}_1^{T,k} \underline{R}^T \underline{B} \left(f^{\text{num},k} \left(\left(\varepsilon_1^k\right)^-, \left(\varepsilon_1^k\right)^+ \right) - \frac{1}{2} \underline{R} \underline{\varepsilon}_1^k \right) \\ &= \frac{\Delta x_k}{2} \left(T^k(u), \varepsilon_1^k \right) + \frac{\Delta x_k}{2} \left(\underline{Q}(u)^k, \underline{\varepsilon}_1^k \right)_{M+\tilde{K}} - \tilde{\varepsilon}_2^k. \end{aligned}$$

We sum over all elements and obtain

$$\begin{aligned} & \frac{1}{2} \frac{d}{dt} \sum_{k=1}^K \frac{\Delta x_k}{2} \|\varepsilon_1^k\|_{M+\tilde{K}}^2 + \sum_{k=1}^K \underline{\varepsilon}_1^{T,k} \underline{R}^T \underline{B} \left(\underline{\varepsilon}_1^{\text{num},k} - \frac{1}{2} \underline{R} \underline{\varepsilon}_1^k \right) \\ &= \sum_{k=1}^K \left(\frac{\Delta x_k}{2} \left(\left(T^k(u), \varepsilon_1^k \right) + \left(\underline{Q}(u)^k, \underline{\varepsilon}_1^k \right)_{M+\tilde{K}} \right) - \tilde{\varepsilon}_2^k \right), \end{aligned} \quad (41)$$

where $\underline{\varepsilon}_1^{\text{num},k} := f^{\text{num},k} \left(\left(\varepsilon_1^k\right)^-, \left(\varepsilon_1^k\right)^+ \right)$. This equation has the same form as (28) except the right side. We estimate the bracket on the right hand side by the Cauchy-Schwarz inequality. It is

$$\begin{aligned} \tilde{R} &= \sum_{k=1}^K \frac{\Delta x_k}{2} \left(\left(T^k(u), \varepsilon_1^k \right) + \left(\underline{Q}(u)^k, \underline{\varepsilon}_1^k \right)_{M+\tilde{K}} \right) \\ &\leq \sqrt{\sum_{k=1}^K \frac{\Delta x_k}{2} \|T^k(u)\|^2} \sqrt{\sum_{k=1}^K \frac{\Delta x_k}{2} \|\varepsilon_1^k\|^2} + \sqrt{\sum_{k=1}^K \frac{\Delta x_k}{2} \|\underline{Q}(u)^k\|_{M+\tilde{K}}^2} \sqrt{\sum_{k=1}^K \frac{\Delta x_k}{2} \|\underline{\varepsilon}_1^k\|_{M+\tilde{K}}^2}. \end{aligned}$$

With the global norm over all elements and the equivalence between the continuous and discrete norms, we obtain

$$\tilde{R} \leq \{c\|T\| + \|Q\|_{\tilde{K}}\} \|\varepsilon_1\|_{\tilde{K}} \equiv \tilde{\mathbb{E}}(t) \|\varepsilon_1\|_{\tilde{K}}, \quad (42)$$

Now, we focus on $\tilde{\varepsilon}_2^k = \left(\varepsilon_1^k \mathbb{I}^N(u)^k \Big|_{-1}^1 - \underline{\varepsilon}_1^{T,k} \underline{R}^T \underline{B} f^{\text{num},k} \left(\mathbb{I}^N(u)^{k,-}, \mathbb{I}^N(u)^{k,+} \right) \right)$ with $\varepsilon_1^k = \mathbb{I}^k(u) - U^k \in \mathbb{P}_N$. ε_1^k is continuous and also uniformly continuous in the compact interval $[-1, 1]$ for all $k \in \{1, \dots, K\}$. \underline{R} is the restriction to the boundaries and $\mathbb{I}^N(u)^k \in \mathbb{P}_N$. The first term can be expressed by $\varepsilon_1^k \mathbb{I}^N(u)^k \Big|_{-1}^1 = \underline{\varepsilon}_1^{T,k} \underline{R}^T \underline{B} \underline{R} \underline{\mathbb{I}^N(u)}^k$, since $\underline{\varepsilon}_1^{T,k} \underline{R}^T$ approximates /interpolates the value at the boundaries -1 and 1 exactly and ε_1^k are uniformly continuous. We may write

$$\left| \tilde{\varepsilon}_2^k \right| = \left| \varepsilon_1^k \mathbb{I}^N(u)^k \Big|_{-1}^1 - \underline{\varepsilon}_1^{T,k} \underline{R}^T \underline{B} f^{\text{num},k} \left(\mathbb{I}^N(u)^{k,-}, \mathbb{I}^N(u)^{k,+} \right) \right|$$

$$\begin{aligned}
&= \left| \underline{\varepsilon}_1^{T,k} \underline{R}^T \underline{B} \underline{R} \underline{\mathbb{I}^N(u)}^k - \underline{\varepsilon}_1^{T,k} \underline{R}^T \underline{B} f^{\text{num},k} \left(\mathbb{I}^N(u)^{k,-}, \mathbb{I}^N(u)^{k,+} \right) \right| \\
&\leq \left| \underline{\varepsilon}_1^{T,k} \underline{R}^T \left(\underline{B} \underline{R} \underline{\mathbb{I}^N(u)}^k - \underline{B} f^{\text{num},k} \left(\mathbb{I}^N(u)^{k,-}, \mathbb{I}^N(u)^{k,+} \right) \right) \right|.
\end{aligned}$$

u is continuous, $\|u\|_{H^m_\varepsilon}$ is uniformly bounded in time, $\mathbb{I}^N(u)^k$ is bounded in every element and so also the numerical flux f^{num} . Therefore, the bracket is bounded.

The absolute value of ε_1^k can be estimate by twice the maximum value and since all norms are equivalent, we are able to estimate every ε_1^k by the global discrete norm. We obtain

$$\sum_{k=1}^K \left| \tilde{\varepsilon}_2^k \right| \leq |Max(t)| \|\varepsilon_1\|_N$$

and altogether

$$\tilde{R} - \sum_{k=1}^N \tilde{\varepsilon}_2^k \leq \left(\tilde{\mathbb{E}}(t) + |Max(t)| \right) \|\varepsilon_1\|_{\tilde{K}} = \mathbb{E}_V(t) \|\varepsilon_1\|_{\tilde{K}}, \quad (43)$$

Remark 4.2. The estimations for $\tilde{\varepsilon}_2^k$ are rough. As we already mentioned before, the error can be seen as an additional dissipation term, which is added in the Gauß-Legendre case. Therefore, a more accurate investigation of this term would be desirable, especially if not a linear problem is analysed, but this is still work in progress. Simultaneously, with inequality (41) and if $0 < \sum_{k=1}^K \tilde{\varepsilon}_2^k$ the Gauß-Legendre error bounds should be less than in the Gauß-Lobatto case. Indeed, our numerical tests demonstrate that all simulations using the Gauß-Legendre nodes lead to more accurate solutions.

Because of the construction of $\tilde{\varepsilon}_2$ and the evaluation at the element boundaries we suppose that ε_1 has a direct influence on ε_2 and we also get some noisy behaviour. In a numerical study we confirm this predictions in the next section 5.

Using estimation (43) in (41), we get an inequality for the global error equation of the total energy. It is

$$\frac{1}{2} \frac{d}{dt} \|\varepsilon_1\|_{\tilde{K}}^2 + \sum_{k=1}^K \underline{\varepsilon}_1^{T,k} \underline{R}^T \underline{B} \left(\underline{\varepsilon}_1^{\text{num},k} - \frac{1}{2} \underline{R} \underline{\varepsilon}_1^k \right) \leq \mathbb{E}_V(t) \|\varepsilon_1\|_{\tilde{K}}. \quad (44)$$

Applying the same approach like in [16] and split the sum into three parts(One for the left physical boundary, one for the right physical boundary and a sum over the internal element endpoints), we get

$$\begin{aligned}
&\sum_{k=1}^K \underline{\varepsilon}_1^{T,k} \underline{R}^T \underline{B} \left(\underline{\varepsilon}_1^{\text{num},k} - \frac{1}{2} \underline{R} \underline{\varepsilon}_1^k \right) = \sum_{k=1}^K \underline{\varepsilon}_1^{T,k} \underline{R}^T \underline{B} \left(f^{\text{num},k} \left((\varepsilon_1^k)^-, (\varepsilon_1^k)^+ \right) - \frac{1}{2} \underline{R} \underline{\varepsilon}_1^k \right) \\
&= -\mathbf{E}_L^1 \left(f_L^{\text{num},1} - \frac{1}{2} \mathbf{E}_L^1 \right) + \sum_{k=2}^K \left(f_L^{\text{num},k} - \frac{1}{2} (\mathbf{E}_R^{k-1} + \mathbf{E}_L^k) \right) (\mathbf{E}_R^{k-1} - \mathbf{E}_L^k) \\
&+ \mathbf{E}_R^K \left(f_R^{\text{num},K} - \frac{1}{2} \mathbf{E}_R^K \right).
\end{aligned}$$

We describe with \mathbf{E}_i ($i = L, R$) the approximated error ε_1 , the indices give the position in the elements, $f_L^{\text{num},k} := f^{\text{num},k}(\mathbf{E}_R^{k-1}, \mathbf{E}_L^k)$, $f_L^{\text{num},1} := f^{\text{num},1}(0, \mathbf{E}_L^1)$ and $f_R^{\text{num},K} := f^{\text{num},K}(\mathbf{E}_R^K, 0)$. The external states for the physical boundary contributions are zero, because $\mathbb{I}^N(u)^1 = g$ at the left boundary and the external state for U^1 is set to g . At the right boundary, where the upwind numerical flux is used, it doesn't matter what we set for the external state, since its coefficient in the numerical solution is zero. We get for the inner

element with $\llbracket \mathbf{E}^k \rrbracket = \mathbf{E}_R^{k-1} - \mathbf{E}_L^k$

$$\sum_{k=2}^K \left(f_L^{\text{num},k} - \frac{1}{2} (\mathbf{E}_R^{k-1} + \mathbf{E}_L^k) \right) (\mathbf{E}_R^{k-1} - \mathbf{E}_L^k) = \sum_{k=2}^K \frac{\sigma}{2} (\llbracket \mathbf{E}^k \rrbracket)^2 \geq 0, \quad \text{with } \begin{cases} \sigma = 0 & \text{central flux,} \\ \sigma = 1 & \text{upwind flux.} \end{cases}$$

For the left and right boundaries, we get finally

$$\begin{aligned} \text{left:} \quad & -\mathbf{E}_L^1 \left(f_L^{\text{num},1} - \frac{1}{2} \mathbf{E}_L^1 \right) = -\mathbf{E}_L^1 \left(\left(\frac{0 + \mathbf{E}_L^1}{2} - \sigma \frac{\mathbf{E}_L^1}{2} \right) - \frac{\mathbf{E}_L^1}{2} \right) = \frac{\sigma}{2} (\mathbf{E}_L^1)^2, \\ \text{right:} \quad & \mathbf{E}_R^K \left(f_R^{\text{num},K} - \frac{1}{2} \mathbf{E}_R^K \right) = \mathbf{E}_R^K \left(\left(\frac{0 + \mathbf{E}_R^K}{2} + \frac{1}{2} \sigma \mathbf{E}_R^K \right) - \frac{\mathbf{E}_R^K}{2} \right) = \frac{\sigma}{2} (\mathbf{E}_R^K)^2. \end{aligned}$$

Therefore, the energy growth rate is bounded by

$$\frac{1}{2} \frac{d}{dt} \|\varepsilon_1\|_{\tilde{K}}^2 + \underbrace{\frac{\sigma}{2} \left((\mathbf{E}_R^K)^2 + (\mathbf{E}_L^1)^2 \right) + \frac{\sigma}{2} \sum_{k=2}^K (\llbracket \mathbf{E}^k \rrbracket)^2}_{BTs} \leq \mathbb{E}_V(t) \|\varepsilon_1\|_{\tilde{K}}. \quad (45)$$

It is $BTs \geq 0$. This is exactly the same form as in [16] and we may estimate/bound similar to [16, 18] the error in time. In the term \mathbb{E}_V , we have an additional term Max , but this has no influence in the estimation here. We now rewrite (45) in the following form:

$$\frac{\partial}{\partial t} \|\varepsilon_1\|_{\tilde{K}} + \underbrace{\frac{BTs}{\|\varepsilon_1\|_{\tilde{K}}^2}}_{\eta(t)} \|\varepsilon_1\|_{\tilde{K}} \leq \mathbb{E}_V(t). \quad (46)$$

Like it was described in [18], we assume that the mean value of $\eta(t)$ over any finite time interval is bounded by a positive constant δ_0 from below. This means that $\bar{\eta} \geq \delta_0 > 0$. Under the assumption for u also the right hand side $\mathbb{E}_V(t)$ is also bounded in time and we can put $\max_{s \in [0, \infty)} \mathbb{E}_V(s) \leq C_1 < \infty$. Applying these facts in (46), we integrate over the time and get the following inequality for the error

$$\|\varepsilon_1(t)\|_{\tilde{K}} \leq \frac{1 - \exp(-\delta_0 t)}{\delta_0} C_1, \quad (47)$$

see [18, Lemma 2.3] for details. We transferred the results from [16, 18] to the more general case of the one parameter family of Vincent et al. [27] and extended the basis also to Gauß-Legendre. We may conclude:

If the truncation error is bounded, the dissipative boundary conditions keep also the error bounded in time for both Gauß-Lobatto as well as Gauß-Legendre nodes. The selections of basis and numerical fluxes have an essential influence on the error behaviour.

It is clear that this approach can be easily transformed to multidimensional problems using a tensor product structure on structured grids.

Remark 4.3. In our investigation, we apply the discrete norms of the one parameter family of Vincent et al. which correspond to some kind of broken Sobolev norms. We assume that c in (12) tends rapidly to zero if we increase the order of accuracy p . With this assumption we include the main used schemes presented in table 1. For the interpolation error we neglect the second part and the first part is estimated by the estimations (21) - (26). Nevertheless, the stability analysis of [27] allows that c can also tend to infinity. Therefore, a more detailed analysis is necessary. We may estimate the second part of the broken Sobolev norm (12) using Bernstein inequality together with estimation (21) or directly (23). Spectral convergence is investigated under the requirement that our solution is C^∞ and m from (23) tends to ∞ for all orders of accuracy. A further investigation about the approximation behaviour concerning a triple limit process of $N, m, c \rightarrow \infty$ would be indeed desirable for this case. But it is beyond the scope of this paper where the influence of the flux functions and nodal bases is investigated.

5 Numerical Tests

In this section we consider numerical tests, which demonstrate error bound (47). In [16, Subsection 6.2], the authors already consider a system for two space dimensions in the DGSEM framework and make equivalent observations like in the one-dimensional setting. Therefore, the more general case gives no further information. This is the reason, why we limit ourself to the one-dimensional case. However, we have a different topic in our investigation. We do not only apply Gauß-Lobatto nodes, but also employ a Gauß-Legendre basis. Our numerical simulations confirm our observation from remark 4.2 that the error term $\tilde{\varepsilon}_2^k$ may have an positive effect on the numerical scheme and we get more accurate solutions by using a Gauß-Legendre basis. Also the influence of the different numerical fluxes is less important as in the Gauß-Lobatto case especially if we chose the SBP-FR methods with $\underline{C} = \underline{M}^{-1} \underline{R}^T \underline{B}$ for the space discretisation.

Simultaneously, results about the error behaviour of several other correction terms \underline{C} will be given. The numerical schemes of table 1 and multiples of them will be considered. We present several examples, which justify our observations, but we show also some limitations of our results.

We use an upwind flux (dotted lines) and central flux (straight lines) at the interior element interfaces¹⁰.

For time integration we use in all numerical examples a SSPRK(3,3) and the time step is chosen in such way that the time integration error is negligible. All elements are of uniform size.

5.1 Error behaviour in One Space Dimension

Sine-Testcase

For comparison reason, we start our numerical section with the same example as in [16]. We analyse the error behaviour for $L = 2\pi$ and the initial condition $u_0 = \sin(12(x - 0.1))$, with the boundary condition $g(t)$ chosen so that the exact solution is $u(x, t) = \sin(12(x - t - 0.1))$. In Figure 1 we illustrate the discrete errors over time for different number of elements with a fourth order polynomial approximation. The errors are always bounded in time for all combinations (upwind/central flux and Gauß-Lobatto/Gauß-Legendre basis). We realise that the upwind flux errors reach in all cases its asymptotic values faster than the central flux errors. Simultaneously, the error bounds for the central flux are larger than for the upwind flux. These results are already formulated in [16] as some predictions (P1 and P2) and also the fact that the central flux errors are noiser than the upwind flux in all observations for all of the meshes and polynomial orders.

Here, we make the following two *new* observations:

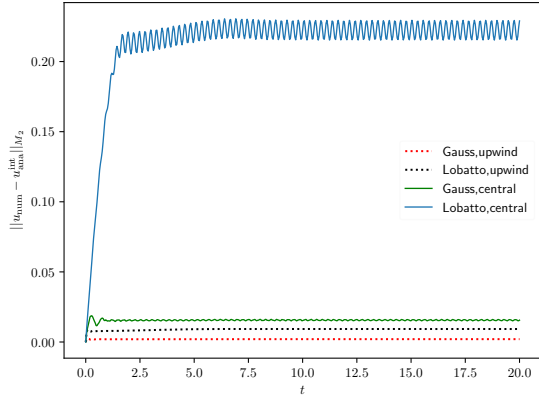
First, the error bounds using Gauß-Lobatto points are larger than in the Gauß-Legendre case and secondly, the influence of the different numerical fluxes is less important than in the Gauß-Lobatto case. The first observation confirms our remark 4.2. The error term $\tilde{\varepsilon}_2$ has an positive effect on the total error and we get a more accurate solution in this case. We interpret that as due to the fact that when using Gauß-Legendre nodes, which do not include the points at the element interfaces, additional dissipation comes from this and the influence of the dissipation from the upwind flux is less important compared to the Gauß-Lobatto case. If we increase the order of approximation, the error bounds of the different combinations should conform. Figure 2 justifies this consideration.

Last, but not least, we study also the convergence speed and observe spectral accuracy in all cases, see Figure 3. This suggest that the approximation errors in $\mathbb{E}(t)$ decay faster than $\frac{1}{\delta_0}$ grows, since with inequality (47) one predicts that the time asymptotic error is bounded by $\mathbb{E}(t)/\delta_0$. This matches also with the investigation in [16].

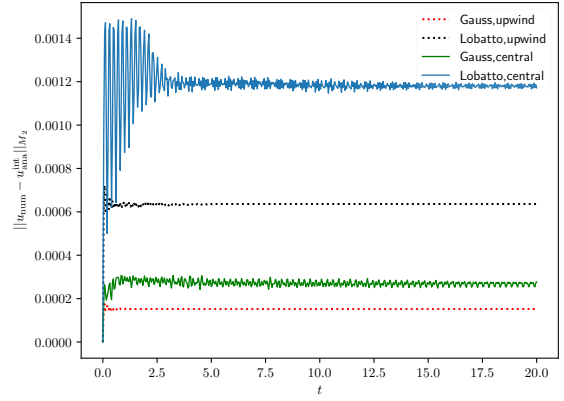
We are not only considering the FR scheme which is equivalent to the DG framework. We also investigate the schemes of Huynh and the SD methods.

The correction terms are written in table 1 and we demonstrate the error behaviours in figure 4 using one time the \tilde{K} -norm and the other time the global norm (19). We realise that the error is always bounded in all cases and, indeed, that the influence of the numerical flux is less important comparing to the chosen basis function. Here, the usage of Gauß-Legendre nodes demonstrates their good advantage comparing to the usage of Gauß-Lobatto nodes. Nevertheless, we make also one more observation in this case. Different from

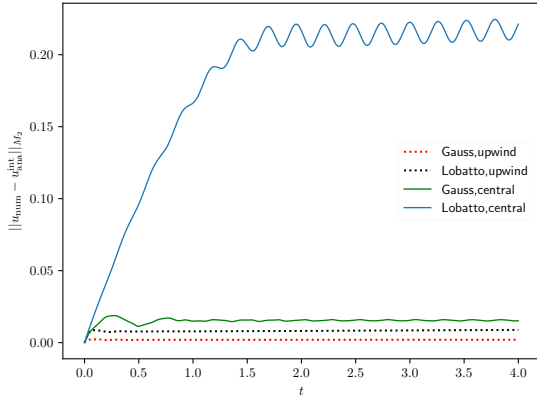
¹⁰We apply always an upwind flux at the physical boundaries.



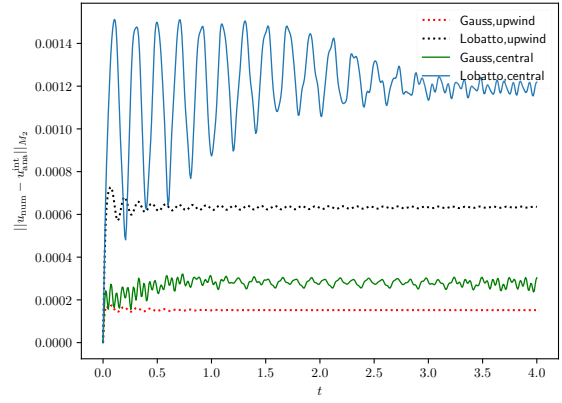
(a) $N = 4, K = 30, t = 20$



(b) $N = 4, K = 50, t = 20$

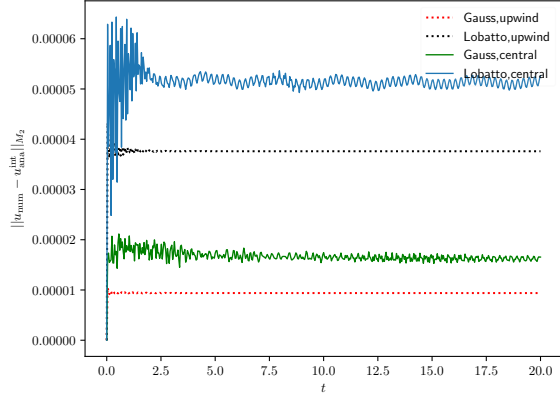


(c) $N = 4, K = 30, t = 4$

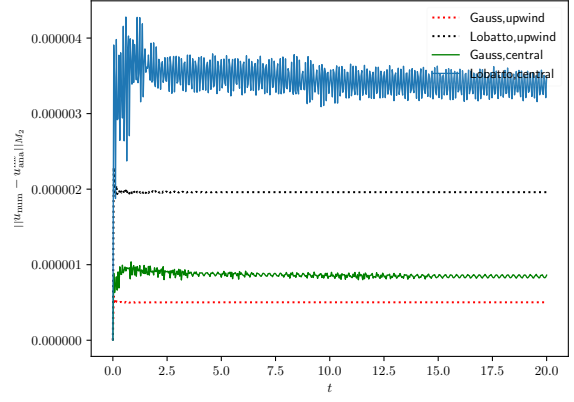


(d) $N = 4, K = 50, t = 4$

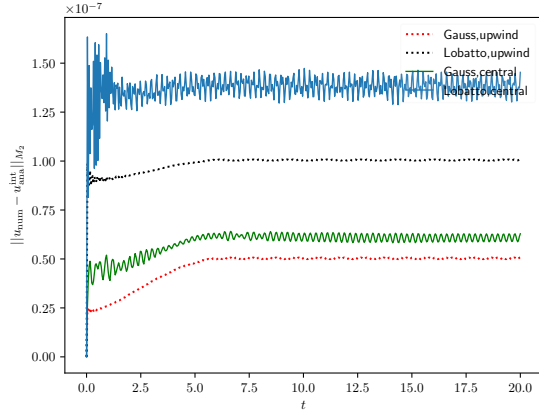
Figure 1: Error as a function in time. The dashed lines are always the calculation with the upwind flux. Right side less elements than right. (c) and (d) early time behaviour.



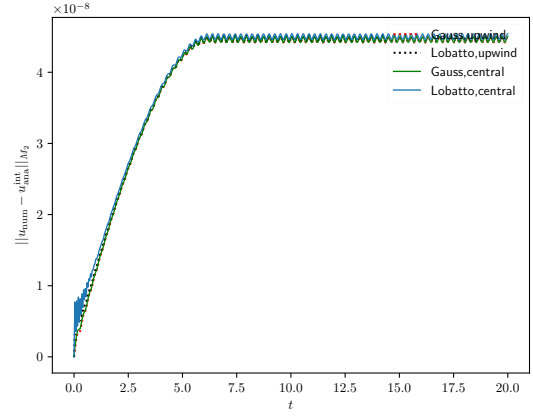
(a) $N = 5$



(b) $N = 6$



(c) $N = 7$



(d) $N = 8$

Figure 2: Error as a function in time. The dashed lines are always the calculation with the upwind flux. $K = 50$ and $t = 20$.

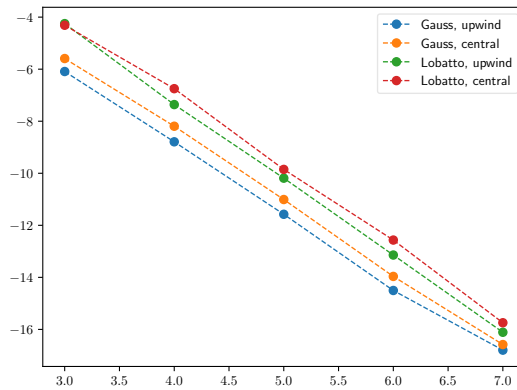
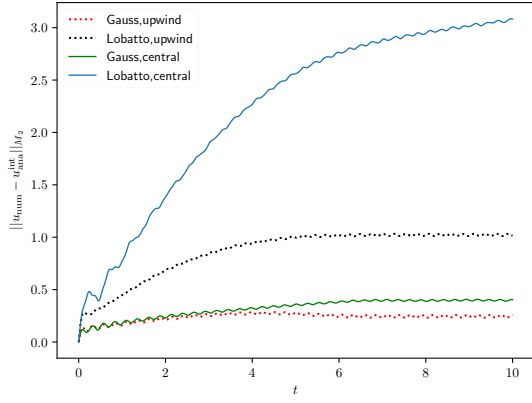
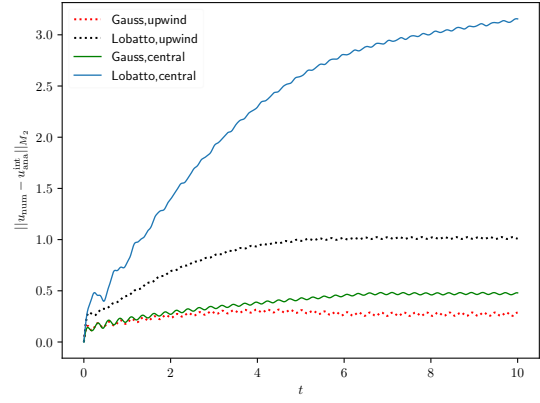


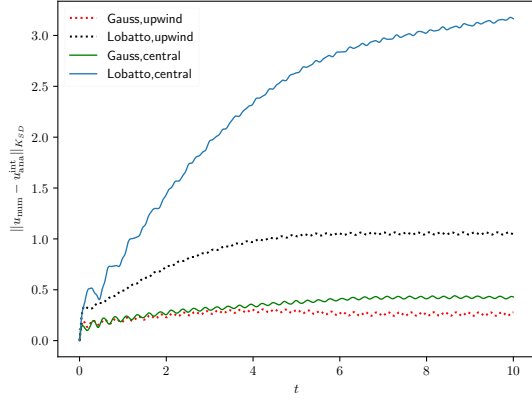
Figure 3: Convergences in time asymptotic errors (last value) as functions of N for $K = 50$.



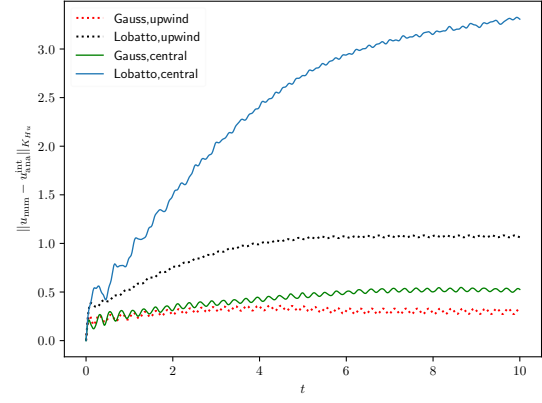
(a) $N = 3, K = 20, t = 10$



(b) $N = 3, K = 20, t = 10$



(c) $N = 3, K = 20, t = 10$



(d) $N = 3, K = 20, t = 10$

Figure 4: Error as a function in time. The dashed lines are always the calculation with the upwind flux. Right side SD scheme and on the left side Huynh. (c) and (d) respective \tilde{K} -norm.

the DG-case our errors show always some oscillations even using the upwind flux. This can be seen in figure 5 where only Gauß-Legendre nodes are considered. This is due to the fact that using another correction term as for the case $c = 0$, we get some *over correction* and *under correction* at the boundaries. It is not surprising that by using Gauß-Lobatto nodes and a central flux we get the worst simulation if the resolution is low order. If we decrease the correction terms more rapidly to zero we get the DG case as the limit. In

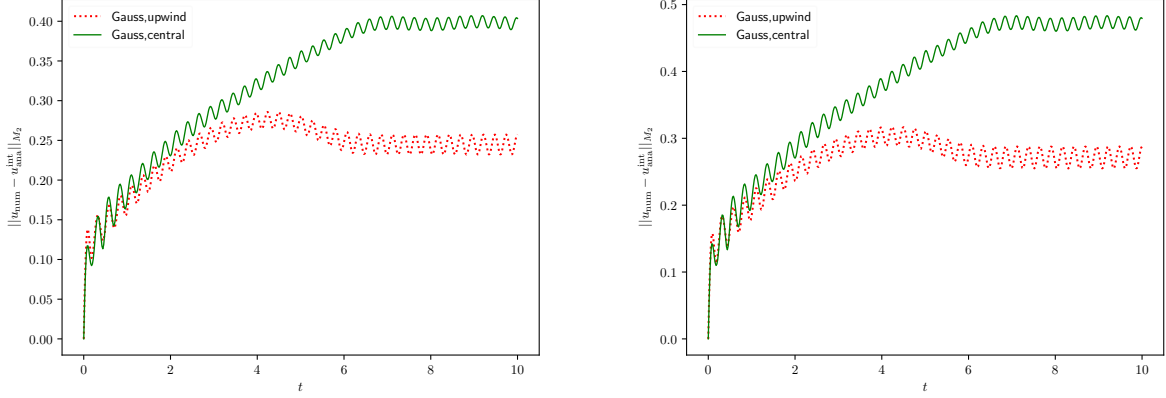


Figure 5: Error as a function in time only with Gauß-Legendre nodes. Left: SD, Right: Huynh

figure 6 we plot the SD method and Huynh scheme by dividing the correction terms with 2^{N-1} . We see that these simulation behaves like 1 expect the noisy behaviours. We also realise that using Gauß-Legendre nodes demonstrates higher oscillations and, therefore, the Gauß-Lobatto nodes seems better (more about this in section 5.2).

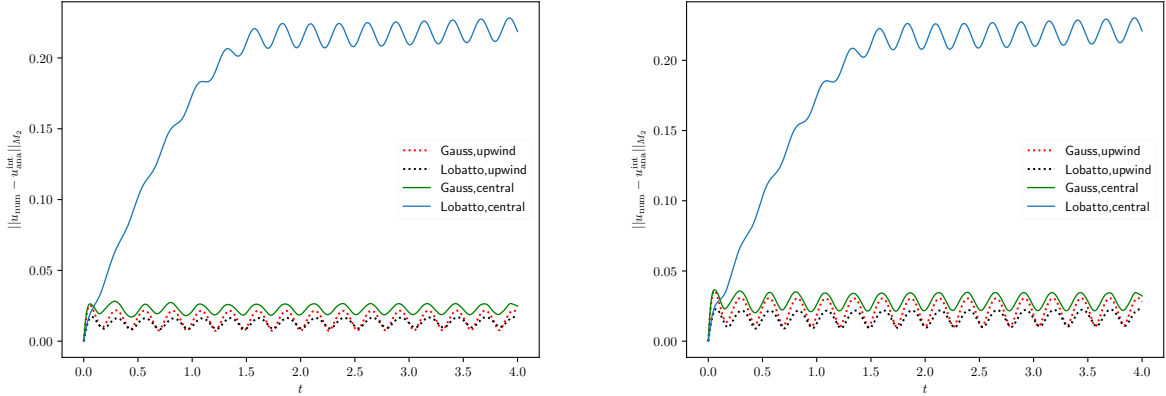


Figure 6: Error as a function in time only with Gauß nodes $K = 30$ and $N = 4$.
Correction Term: $c_{SD}/2^{N-1}$ (left), $c_{Hu}/2^{N-1}$ (right)

Cosine-testcase

As a second test case, we investigate the error behaviour for $L = 2\pi$ and the initial condition $u_0 = \cos(12(x - 0.1))$, with the boundary condition $g(t)$ chosen so that the exact solution is $u(x, t) = \cos(12(x - t - 0.1))$. With this test case we want to strengthen our results from before.

In Figure 7 we illustrate the discrete errors over time for different number of elements with a fourth and sixth order polynomial approximation. We make equivalent observations like before and see that using

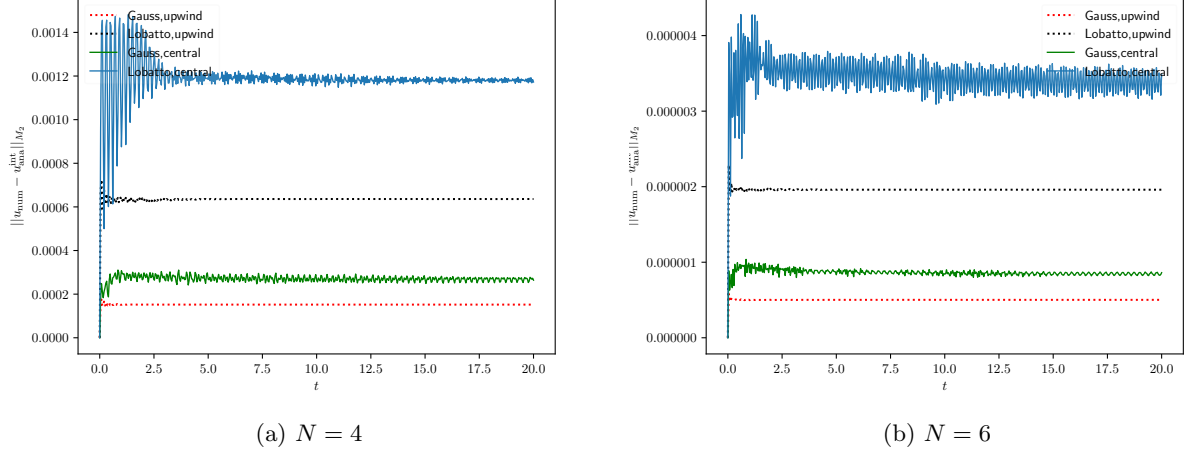


Figure 7: Error as a function in time with 50-elements.

Gauß-Legendre nodes in our scheme yields to more accurate solutions as Gauß-Lobatto nodes. Also the difference between the upwind flux error and central flux error is not so large. The same observations can be made by using the FR schemes from before.

$\tilde{\varepsilon}_2$ -term

Finally, we have a short look on the $\tilde{\varepsilon}_2$ terms for the two test cases. In figure 8 the $\tilde{\varepsilon}_2$ -error is plotted over the time for different polynomial orders in the sin test case. Both times the error starts positive for the lower

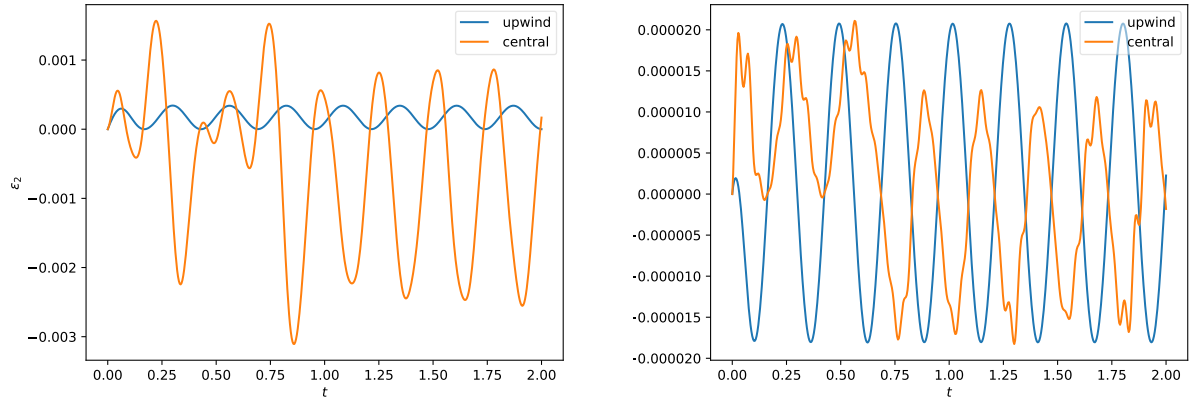


Figure 8: $\tilde{\varepsilon}_2$ a function in time $K = 30$ and $N = 4, 5$.

order approximation ($N = 4$) and the upwind flux stays strictly positive whereas the term using the central flux shows higher oscillations and turns also negative. Even the middle point of the amplitudes is below zero. Since the ε_1 -errors show these oscillations applying the central flux we also get them in the $\tilde{\varepsilon}_2$ -terms. This is also not surprising since ε_1 has a direct influence on $\tilde{\varepsilon}_2$. Using a fifth order approximation the amplitude

using the upwind flux shows an higher amount, but these are symmetrical around zero whereas applying the central flux the symmetric point lies in the negative axis. Comparing the amounts of the total error in figure 1 with these demonstrates that the $\tilde{\varepsilon}_2$ errors is significantly less, but may have an positive influence especially if Gauß-Legendre nodes are used. In Figure 9 we have an analogous behaviour for the cosine test case. All of these strengthen our investigation/observation from before.

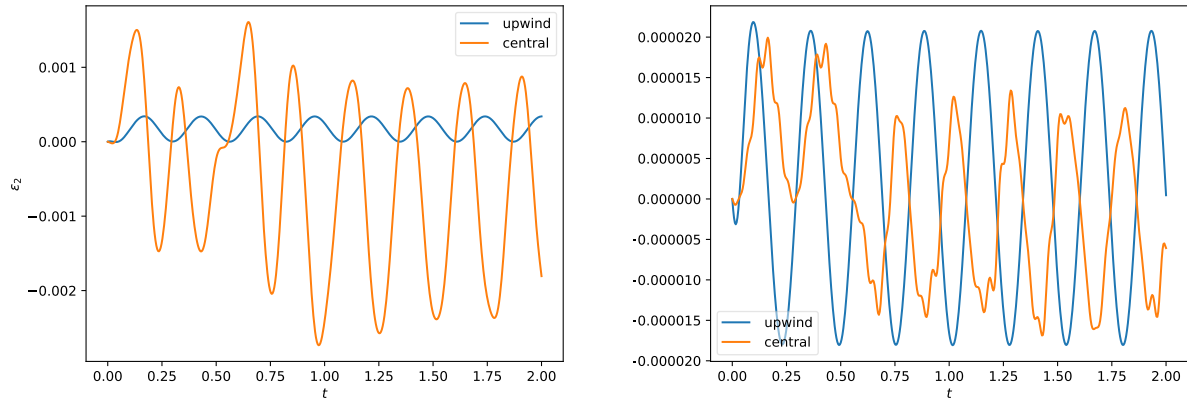


Figure 9: $\tilde{\varepsilon}_2$ a function in time $K = 30$ and $N = 4, 5$.

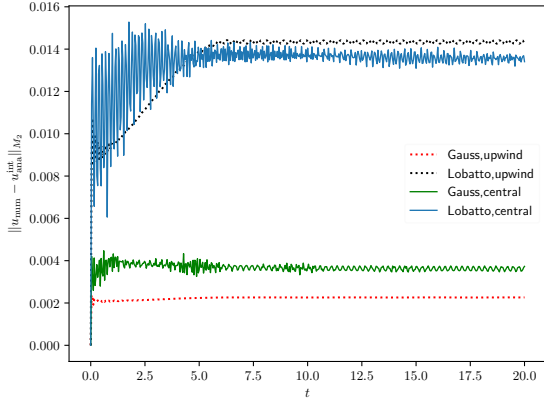
5.2 Limitations and Counterexamples

We make a series of test calculations and most of the time, we make the above observations. Nevertheless there are several examples, which qualify our results and also some predictions of [16]. At first, we concentrate on the FR scheme which is equivalent to the DG framework and can be seen as the limit process of several FR schemes. We demonstrate and interpret these examples.

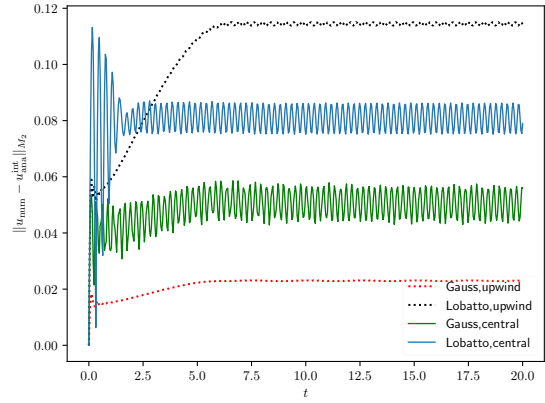
In the error plot 3, one may realise that the upwind error lies under the central error if a polynomial approximation of order three is used. In fact, we see this clearly in Figure 10 (a). Here, the central error lies above the upwind error and also the asymptotic state is nearly the same¹¹. We may interpret this that using polynomial order 3 in our schemes is too inaccurate for the approximation with the Gauß-Lobatto basis. Then, with applying an upwind flux yields too much dissipation into our calculation and we get this unpredictable behaviour, which damps our observation from above and also some predictions from [16]. In Figure 10 (b), we get a similar error behaviour as before, if we decrease the number of elements¹² K . With the higher jumps at the element interfaces the upwind flux yields to a more inexact numerical solution. We may conclude that we need an adequate number of elements to get the predicted results in the Gauß-Lobatto case. However, the numerical errors (upwind and central) with the Gauß-Legendre basis show the suspected behaviours from our results and one may interpret that as an advantage by using these type of basis, but this is a little bit misleading. In Figure 11 (a) we see the numerical errors of the cosine-case if we use polynomial order 3 and 20 elements. Here, the errors using Gauß-Lobatto basis show the expected manner and the errors with Gauß-Legendre basis do not. We assume that by using Gauß-Legendre basis and an upwind flux the jumps between the element interfaces is too high and we get this effect. If we again increase the number of elements and so the degrees of freedom, we realise a change in the error behaviours, compare 11 (a)-(c). Nevertheless, the absolute error values by using Gauß-Legendre nodes are comparatively low. This limitation are noticed by focusing on the scheme with correction matrix (7) which can be seen as the limit process of the other schemes. As it is already known [5, 27, 28], the most accurate results are obtained

¹¹We assume that the noisy state is *periodic* with the central flux.

¹²In [8] the influence of the dispersion and dissipation errors of Gauß-Legendre and Gauß-Lobatto is investigate also in respect to the number of elements.

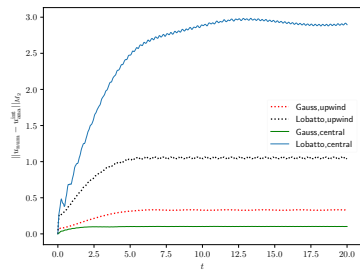


(a) $N = 3, K = 50, t = 20$

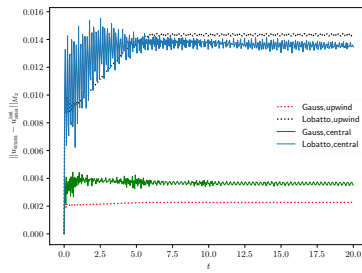


(b) $N = 4, K = 20, t = 20$

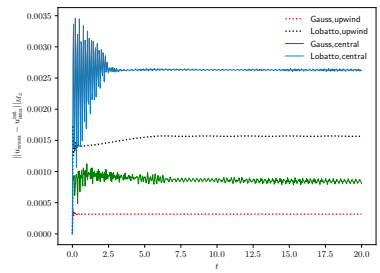
Figure 10: Error as a function in time.



(a) $N = 3, K = 20, t = 20$



(b) $N = 3, K = 50, t = 20$



(c) $N = 3, K = 80, t = 20$

Figure 11: Error as a function in time.

if $c = 0$.

Nevertheless, for other correction terms we have also some limitations for our predictions. Already in figure 6 we realise that error using Gauß-Lobatto nodes and an upwind flux is less compared to the Gauß nodes, since the amplitude of the oscillations are not so big. Indeed, for FR schemes with $c \neq 0$ we have some over and under corrections at the boundaries of every element. If we increase the order or accuracy these amplitude will decrease and, since the Gauß-Lobatto nodes work at the boundaries, it will yield to an error which is equal or less than using Gauß-Legendre nodes. Simultaneously, we have to realise that using Gauß-Legendre lead already in low order computations are comparatively good error behaviours, compare figures 6 and 12.

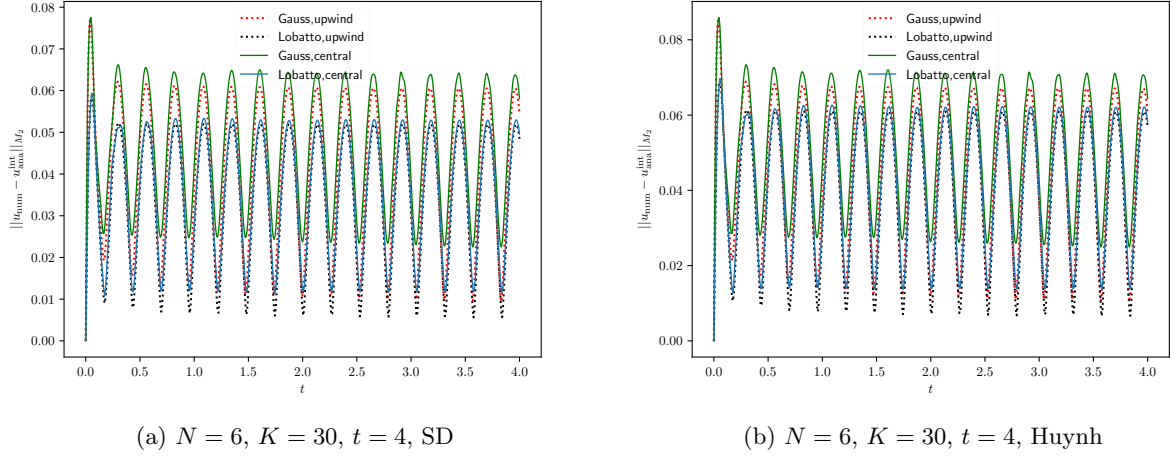


Figure 12: Error as a function in time.

Already in section 3 we mentioned to present an example, where the norm of solution $\|u\|_{H_c^m}$ is not uniform bounded in time. We select our initial and boundary conditions in such way, that we get as the solution $u(t, x) = (x - t)^8$. Figure 13 demonstrates the unbounded increase of the error for different times.

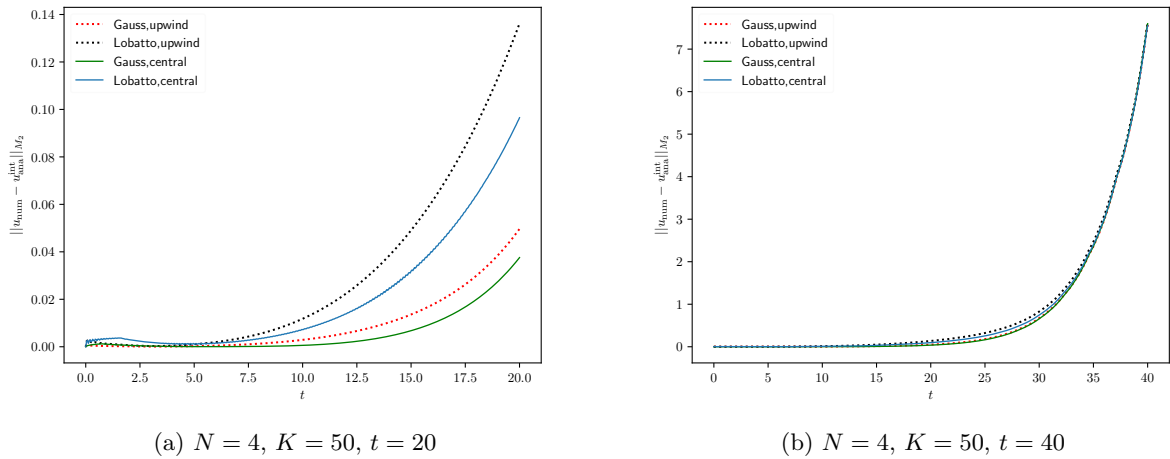


Figure 13: Error as a function in time.

6 Summary and Conclusion

In this paper, we transfer the results about the bounded error growth from the discontinuous Galerkin spectral element method [16] to the more general framework of SBP-FR methods. Furthermore, we extend the investigation by including the Gauß-Legendre basis, where [16] considers only the Gauß-Lobatto basis. Indeed, for both bases (Gauß-Lobatto /Gauß-Legendre), the numerical flux used at element boundaries affects the error growth behaviour. If an adequate number of elements is used, the upwind flux leads to better results. The asymptotic values are smaller and are reached in a shorter time period. At once, also the selection of basis has a big influence and in our opinion is even more important. Using Gauß-Legendre basis, the error reaches the asymptotic value faster and to a lower value than by using Gauß-Lobatto basis. Also, the impact of the different numerical fluxes (central/ upwind) is by applying Gauß-Legendre basis less important as in the Gauß-Lobatto case, especially using a low order polynomial approximation. These effects decrease when the order of polynomial approximation is increased and/or using more elements (which also increase the resolution).

The investigation implies that the usage of Gauß-Legendre basis has some advantages compared to Gauß-Lobatto and should be preferred. However, there are several points, which we have to mention yet.

We investigate a trivial model problem (14), where the flux function is simple $f(u) = u(x, t)$. Already by using the more complicated flux $f(u) = a(x)u(x, t)$ several problems arises in the discretisation by using Gauß-Legendre nodes, see [17] for details. The reason is that Gauß-Legendre points do not include the boundary points in one element, and we get some aliasing effect if we are not careful in the discretisation. In [24], the author proves a way to solve these issues by applying further correction terms to approximate the boundary terms correctly. For non-linear flux functions stability problems rise automatically. The aliasing effect is quite stronger and to remedy these issues, further correction terms are needed [25]. By including the boundary points, these correction terms are simpler and better understand. [23] provides the correction terms for the shallow water equation using Gauß-Legendre nodes, but to this point it is not clear how to construct these terms for more complicated equations like Euler-equation. In our calculations, the time integration analysis was negligible, but in real time simulation and practical use it is also an important issue. In [8], the authors already investigate the time-step restriction by using Gauß-Lobatto or Gauß-Legendre nodes in the DGSEM and find out that Gauß-Lobatto nodes have favoured properties.

The above mentioned issues are not unimportant. However, for linear problems with adequate initial conditions the usage of Gauß-Legendre basis should be taken into account. In our tests, the asymptotic error values are always reached faster and to a smaller amount. Nevertheless, further studies are necessary. First, one has to analyse the impact of $\tilde{\varepsilon}_2$ not only numerically but also analytically. Secondly, what happens with the approximation error if the initial conditions have jumps or even more complex flux functions are considered.

References

- [1] S. Abarbanel, A. Ditkowski, and B. Gustafsson. On error bounds of finite difference approximations to partial differential equations—temporal behavior and rate of convergence. *Journal of Scientific Computing*, 15(1):79–116, 2000.
- [2] C. Bernardi and Y. Maday. Properties of some weighted sobolev spaces and application to spectral approximations. *SIAM journal on numerical analysis*, 26(4):769–829, 1989.
- [3] C. Bernardi and Y. Maday. Polynomial interpolation results in sobolev spaces. *Journal of computational and applied mathematics*, 43(1-2):53–80, 1992.
- [4] C. Canuto, M. Y. Hussaini, A. M. Quarteroni, A. Thomas Jr, et al. *Spectral methods in fluid dynamics*. Springer Science & Business Media, 2012.
- [5] P. Castonguay, P. E. Vincent, and A. Jameson. A new class of high-order energy stable flux reconstruction schemes for triangular elements. *Journal of Scientific Computing*, 51(1):224–256, 2012.
- [6] G. Cohen, X. Ferrieres, and S. Pernet. A spatial high-order hexahedral discontinuous galerkin method to solve maxwell’s equations in time domain. *Journal of Computational Physics*, 217(2):340–363, 2006.

- [7] D. Funaro. *Polynomial approximation of differential equations*, volume 8. Springer Science & Business Media, 2008.
- [8] G. J. Gassner and D. A. Kopriva. A comparison of the dispersion and dissipation errors of Gauss and Gauss-Lobatto discontinuous Galerkin spectral element methods. *SIAM Journal on Scientific Computing*, 33(5):2560–2579, 2011.
- [9] J. Hesthaven and R. Kirby. Filtering in legendre spectral methods. *Mathematics of Computation*, 77(263):1425–1452, 2008.
- [10] J. S. Hesthaven and T. Warburton. Nodal high-order methods on unstructured grids: I. time-domain solution of maxwell’s equations. *Journal of Computational Physics*, 181(1):186–221, 2002.
- [11] H. Huynh. A flux reconstruction approach to high-order schemes including discontinuous Galerkin methods. *AIAA paper*, 4079:2007, 2007.
- [12] H. Huynh, Z. J. Wang, and P. E. Vincent. High-order methods for computational fluid dynamics: A brief review of compact differential formulations on unstructured grids. *Computers & Fluids*, 98:209–220, 2014.
- [13] A. Jameson. A proof of the stability of the spectral difference method for all orders of accuracy. *Journal of Scientific Computing*, 45(1-3):348–358, 2010.
- [14] U. Koley, S. Mishra, N. H. Risebro, and M. Svärd. Higher order finite difference schemes for the magnetic induction equations. *BIT Numerical Mathematics*, 49(2):375–395, 2009.
- [15] D. A. Kopriva and G. J. Gassner. On the quadrature and weak form choices in collocation type discontinuous Galerkin spectral element methods. *Journal of Scientific Computing*, 44(2):136–155, 2010.
- [16] D. A. Kopriva, J. Nordström, and G. Gassner. Error boundedness of discontinuous galerkin spectral element approximations of hyperbolic problems, 2016.
- [17] J. Manzanero, G. Rubio, E. Ferrer, E. Valero, and D. A. Kopriva. Insights on aliasing driven instabilities for advection equations with application to gauss-lobatto discontinuous galerkin methods. *arXiv preprint arXiv:1705.01503*, 2017.
- [18] J. Nordström. Error bounded schemes for time-dependent hyperbolic problems. *SIAM Journal on Scientific Computing*, 30(1):46–59, 2007.
- [19] J. Nordström. A roadmap to well posed and stable problems in computational physics. *Journal of Scientific Computing*, 71(1):365–385, 2017.
- [20] J. Nordström and R. Gustafsson. High order finite difference approximations of electromagnetic wave propagation close to material discontinuities. *Journal of Scientific Computing*, 18(2):215–234, 2003.
- [21] P. Öffner. *Zweidimensionale klassische und diskrete orthogonale Polynome und ihre Anwendung auf spektrale Methoden zur Lösung hyperbolischer Erhaltungsgleichungen*. PhD thesis, TU Braunschweig, 2015.
- [22] P. Öffner and T. Sonar. Spectral convergence for orthogonal polynomials on triangles. *Numerische Mathematik*, 124(4):701–721, 2013.
- [23] H. Ranocha. Shallow water equations: Split-form, entropy stable, well-balanced, and positivity preserving numerical methods. *GEM – International Journal on Geomathematics*, 8(1):85–133, 04 2017.
- [24] H. Ranocha. Generalised summation-by-parts operators and variable coefficients. *Journal of Computational Physics*, 362:20–48, 02 2018.
- [25] H. Ranocha, P. Öffner, and T. Sonar. Summation-by-parts operators for correction procedure via reconstruction. *Journal of Computational Physics*, 311:299–328, 2016.
- [26] H. Ranocha, P. Öffner, and T. Sonar. Extended skew-symmetric form for summation-by-parts operators and varying jacobians. *Journal of Computational Physics*, 342:13–28, 2017.
- [27] P. E. Vincent, P. Castonguay, and A. Jameson. A new class of high-order energy stable flux reconstruction schemes. *Journal of Scientific Computing*, 47(1):50–72, 2011.
- [28] P. E. Vincent, A. M. Farrington, F. D. Witherden, and A. Jameson. An extended range of stable-symmetric-conservative flux reconstruction correction functions. *Computer Methods in Applied Mechanics and Engineering*, 296:248–272, 2015.